Miniaturized metabolomics methods for enabling the study of biomass-restricted samples

He, B.

Chapter III

Quantification of endocannabinoids in human cerebrospinal fluid using a novel micro-flow liquid chromatography-mass spectrometry method

Based on:

Bingshu He*, Xinyu Di*, Faisa Guled, Aster V.E. Harder, Arn M.J.M. van den Maagdenberg, Gisela M. Terwindt, Elke H.J. Krekels, Isabelle Kohler, Amy Harms, Rawi Ramautar, Thomas Hankemeier,

Quantification of endocannabinoids in human cerebrospinal fluid using a novel micro-flow liquid chromatography-mass spectrometry method

Analytica Chimica Acta 2022; DOI: 10.1016/j.aca.2022.339888

*Authors contributed equally

Abstract

The endocannabinoid system (ECS) is implicated in various brain disorders. Changes in the composition of the cerebrospinal fluid (CSF) may be associated with ECS-related pathologies. Endocannabinoids (eCBs) and their analogues are present at low concentrations in human CSF, which hampered the investigation of the ECS in this body fluid. In this study, we developed a highly sensitive and selective micro-flow liquid chromatography-tandem mass spectrometry (micro-LC-MS/MS) method for the analysis of eCBs and eCB analogues in human CSF. The developed method allowed for the quantitative analysis of 16 eCBs and their analogues in human CSF. Micro-LC-MS/MS analyses were performed at a flow-rate of 4 µL min^{-1} with a 0.3-mm inner diameter column. A minor modification of a novel spray needle was carried out to improve the robustness of our method. By using an injection volume of 3 µL, our method reached limits of detection in the range from 0.6 to 1293.4 pM and limits of quantification in range from 2.0 to 4311.3 pM while intra- and interday precisions were below 13.7%. The developed workflow was successfully used for the determination of eCBs in 288 human CSF samples. It is anticipated that the proposed approach will contribute to a deeper understanding of the role of ECS in various brain disorders.

1. Introduction

The endocannabinoid system (ECS) is a widely distributed signaling system in the brain, involving cannabinoid receptors 1 and 2 (CB1 and CB2) and their best known endogenous agonists N-arachidonoyl ethanolamine (anandamide, AEA) and 2-arachidonoyl glycerol (2-AG), which are defined as endocannabinoids (eCBs) [1]. Besides AEA and 2-AG, other structural analogues, i.e., other N-acyl ethanolamines (NAEs) and other 2-acylglycerols play important roles in ECS signaling, by enhancing the effects of AEA and 2-AG via increasing receptor affinity or inhibiting hydrolysis, known as the 'entourage effect' [2, 3].

Alterations in the ECS have been reported in experimental models of various brain disorders, including Alzheimer's disease, Parkinson's disease, and migraine [4-7]. To certain extent, the reported findings were supported by those obtained in clinical studies [8-10]. However, most of the clinical studies used plasma or postmortem tissue samples, which limits the validity of ECS findings. Due to its close connection with brain tissue, cerebrospinal fluid (CSF) represents a more suitable biospecimen. Indeed, CSF reflects the level of metabolites in brain and is thus believed to better capture the brain's neurochemistry compared to blood. However, eCBs and their analogues in human CSF, especially AEA, are present at concentrations lower than picomolar or even femtomolar range [11-17], highlighting the need for adequate methods to reliably detect and quantify these compounds [18-20]. In studies reporting endogenous concentrations of eCBs and eCB analogues in human CSF [14-17, 20, 21], relatively large volumes of CSF (≥1 mL) were needed to reach the required sensitivity.

Using low-flow rate ranges between 1 and 50 µL min^{-1}, micro-flow LC leads to the formation of smaller and more uniform spray droplets during the electrospray ionization process, improving the ionization efficiency significantly. Moreover, with the smaller inner diameter columns that are typically used (75 µm to 1 mm-I.D.), micro-flow LC-MS provides higher sensitivity using lower amounts of sample. Since human CSF samples are difficult to obtain, a more sensitive method to make optimal use of such samples is required. Kantae *et al*. [19] developed a quantitative method based on a chip-based nano-LC-MS system for the analysis of eCBs in CSF. Using only 200 µL of human CSF, the method provided a limit of detection (LOD) from 0.3 to 61.2 pM. Intra- and inter-assay variability

(expressed by the coefficient of variation, CV) varied from 2-23% and 3-21%, respectively. However, due to the small inner diameter of the spray emitter, the LC tubing, and the column, the overall stability of such chips remains a challenging aspect in nano-flow LC-MS, contrary to conventional methods with 2.1-mm columns and milliliter range flow rates [22, 23]. In addition, the chips used in the study of Kantae *et al*. are no longer commercially available, showing the need for an alternative method.

In this study, we developed a sensitive and robust micro-LC-MS/MS method for the simultaneous absolute quantification of eCBs and their analogues in human CSF. To improve robustness, the spray needle in the commercial micro spray ion source was modified to avoid clogging. The overall sensitivity was compared between conventional and micro-flow rates. Parameters were optimized for several flow rates and a final method using 4 µL min^{-1} as flow rate and a 0.3-mm inner diameter column was selected. The method was validated based on the guidance of bioanalytical method validation from EMA (2009) [24] for the quantification of eCBs. The validated method was applied to 288 human CSF samples with acceptable performance metrics, thereby demonstrating the value of this method for future studies focusing on deciphering the involvement of ECS in brain disease.

2.Material and methods

2.1 Chemicals and materials

LC-MS-grade acetonitrile (ACN) and formic acid were purchased from Biosolve B.V. (Valkenswaard, Netherlands). Anhydrous methyl tert-butyl ether (MTBE, ≥99.8%), ammonium acetate (≥99.0%) and ammonium formate (≥99.9%) were purchased from Sigma-Aldrich (St. Louis, Missouri, United States). Purified water was obtained from a Milli-Q PF Plus system (Merck Millipore, Burlington, Massachusetts, United States).

The standard reagents α-linolenoyl ethanolamide (α-LEA), palmitoleoyl ethanolamide (POEA), pentadecanoyl ethanolamide (PDEA), linoleoyl ethanolamide (LEA), anandamide (AEA), docosahexaenoyl ethanolamide (DHEA), 1-arachidonoylglycerol (1-AG), 2-arachidonoylglycerol (2-AG), 1-linoleoyl glycerol (1-LG), 2-linoleoyl glycerol (2-LG), palmitoyl ethanolamide (PEA), dihomo-γ-linolenoyl ethanolamide (DGLEA), docosatetraenoyl ethanolamide (DEA), 1-oleoyl glycerol (1-OG), 2-oleoyl glycerol (2-OG),

stearoyl ethanolamide (SEA), eicosapentaenoyl ethanolamide (EPEA), mead acid ethanolamide (ETAEA), N-oleoylethanolamine (OEA) and deuterated standards N-(2-hydroxyethyl-1,1,2,2-d_4)-9Z,12Z-octadecadienamide (LEA-d_4), N-(2-hydroxyethyl-1,1',2,2'-d_4)-4Z,7Z,10Z,13Z,16Z,19Z-docosahexaenamide (DHEA-d_4), N-(2-hydroxyethyl)-5Z,8Z,11Z,14Z-eicosatetraenamide-5,6,8,9,11,12,14,15-d_8 (AEA-d_8), 5Z,8Z,11Z,14Z-eicosatetraenoic-5,6,8,9,11,12,14,15-d_8 acid (2-AG-d_8), N-(2-hydroxyethyl)-hexadecanamide-7,7,8,8-d_4 (PEA-d_4), N-(2-hydroxyethyl)-octadecanamide-18,18,18-d_3 (SEA-d_3) and N-(2-hydroxyethyl-1',1,2,2'-d_4)-9Z-octadecenamide (OEA-d_4) were purchased from Cayman Chemical (Ann Arbor, Michigan, United States).

2.2 Preparation of standards and internal standards solutions

Pure standards (>98% purity) at different stock concentrations were dissolved in ethanol or ACN. The standard stock solutions were diluted to 1 mM using ACN. Standard solution I, used for direct infusion experiments, included 5 nM of each compound in group A (AEA, DEA, DGLEA, DHEA, ETAEA, LEA, EPEA, PDEA, POEA and α-LEA), 50 nM of each compound in group B (2-AG, 1-AG, SEA, OEA, and PEA) and 500 nM of each compound in group C (2-LG, 1-LG, 2-OG, 1-OG). Standard solution II was obtained by diluting standard solution I four times with ACN and used for LC-MS method development.

The deuterated internal standard (ISTD) working solution containing 225.3 nM 2-AG-d_8, 4.5 nM AEA-d_8, 0.6 nM DHEA-d_4, 3.0 nM LEA-d_4, 6.0 nM OEA-d_4, 0.6 nM PEA-d_4 and 12 nM SEA-d_3 was prepared in ACN. All the standard solutions were stored at -20 °C.

2.3 Preparation of calibrant solutions

Table 1. Concentrations of eCBs and eCB analogues standards in calibrant solutions.

Compound group	Concentration (pM)									
	C0	C1	C2	C3	C4	C5	C6	C7	C8	C9
A	0	7.3	14.65	29.3	58.6	117.2	468.8	1875	3750	7500
B	0	73.3	146.5	293.0	586.0	1171.9	4687.5	18750	37500	75000
C	0	732.4	1464.9	2929.7	5859.4	11718.8	46875	187500	375000	750000

Each standard stock solution (1 mM) was mixed and diluted in ACN, resulting in nine calibration concentration levels. For each calibration level, 10 µL of each solution was

mixed with ISTD working solution to reach the adequate concentration. The concentrations of ISTDs were chosen to be in the middle of the dynamic range, i.e., equivalent to C4 concentration. Final concentrations of all compounds are shown in **Table 1**.

2.4 Collection of human CSF samples

CSF samples were collected via a lumbar puncture (LP) in a randomized fashion between 2008 and 2016 and between 9:00 am and 1:00 pm to minimize diurnal and seasonal variation. The protocol was approved by the ethics committee of Leiden University Medical Center. The LP was performed between the L3/L4, L4/L5 or L5/S1 interspace, whereby 3 mL CSF was sampled directly in a 15-mL polypropylene Falcon tube (Cat. No. 188271; Greiner) that already contained 6 mL of cold ethanol and was placed in an ice bath. Ethanol was used to stabilize the metabolites during long-term storage. After the collection of CSF, the tube was gently shaken and immediately put back on ice. Subsequently, the CSF was divided in aliquots of 1.5 mL in 1.8-mL cryotubes (Art. No. 368632; NUNC Brand). The cryotubes were placed on dry ice within 40 min of sampling and immediately transferred to -80°C. All CSF samples remained at -80°C until analysis.

2.5 Sample preparation

The sample preparation was carried out using 750 µL of the mixture of CSF and ethanol (including 500 µL ethanol). Samples were evaporated using a SpeedVac (Thermo Fisher, USA) for 90 min to remove ethanol. Next, 1 mL of MTBE, 50 µL 0.1 M ammonium acetate solution at pH 4 buffer solution and 10 µL ISTD working solution were added to each sample, followed by 10 min of standard vortex and centrifugation. After 5 min, the organic layer was transferred to a 1.5-mL Eppendorf tube and evaporated to dryness. Samples were reconstituted in 20 µL of a mixture of water/ACN (1:1, v/v), vortexed for 20 min and centrifuged at 16,000g for 10 min. Finally, 15 µL of supernatant was transferred in an autosampler vial and injected into the LC-MS instrument.

2.6 Optimization of micro-flow rates and comparison with UHPLC-MS

During the performance comparison evaluation of different flow rates, direct infusion to mass spectrometer and LC-MS methods were used. Direct infusion MS was performed using a syringe pump connected to SCIEX QTRAP 6500+ mass spectrometer (SCIEX,

Framingham, Massachusetts, United States). A Shimadzu Nexera X2 LC-30AD system (Shimadzu corporation., Kyoto, Japan) and Waters nanoAcquity LC system (Waters, Milford, Massachusetts, United States) were used for high- and micro-flow rates, respectively. Various columns and ionization sources suited for each flow rate were chosen to allow for an adequate comparison (**Table 2**). Moreover, UHPLC-MS/MS and micro-LC-MS/MS parameters in this comparison experiment were also optimized for each flow rate and can be found in **Supplemental Table S1**.

Table 2. Experimental conditions used for performance comparison of different flow rates.

	Conventional flow		**Micro-flow**	
Flow rate	550 µL min^{-1}	250 µL min^{-1}	100 µL min^{-1}, 50 µL min^{-1}	1-4 µL min^{-1}
Syringe pump	Harvard Apparatus Model 22			
Syringe (for direct infusion)	Hamilton Gastight #1001			Hamilton Gastight #1750
LC	Shimadzu Nexera X2 LC-30AD			Waters nanoAcquity
Column	Waters BEH C18 (1.7 µm, 2.1 × 50 mm)		Waters HSS T3 C18 (1.8 µm, 1 × 100 mm)	Phenomenex C18 (2.6 µm, 0.3 × 50 mm)
Ionization source (for both direct infusion and LC-MS analysis)	SCIEX Turbo V with a 100-µm I.D. emitter	SCIEX Turbo V with a 100-µm I.D. emitter	SCIEX Turbo V with a 50-µm I.D. emitter	SCIEX nanosprayIII with a 30-µm I.D. emitter

2.7 Micro-LC-MS/MS instrumentation and conditions

The micro-LC-MS/MS analyses were performed using a Waters nanoAcquity LC instrument coupled to a Shimadzu LCMS-8060 triple quadrupole mass spectrometer equipped with a micro-ionization source (Shimadzu corporation., Kyoto, Japan) and an optimized spray needle, i.e., 15-cm Metal TaperTip™ emitter with 30-µm tip inner diameter (New Objective, Littleton, Massachusetts, United States). The separation was carried out using a Phenomenex C18 column (2.6 µm, 0.3×150 mm) maintained at 45°C. The injection volume was 3 µL. Eluent A was composed of 2 mM ammonium formate with 10 mM formic acid in water, and eluent B was ACN. Using a flow rate of 4 µL min^{-1}, the initial gradient started at 55% eluent B and maintained for 0.5 min, eluent B was increased to 60% from 0.5 to 1.5 min, increased to 70% from 1.5 to 2.0 min, to 85% from 2.0 to 5.5 min, and increased to 95% at 5.6 min, where the gradient was kept until 8.0 min, then decreased to

55% eluent B at 8.1 min. The column was equilibrated for 8 min until the next injection, giving a total analysis time of 16 min. MS data was acquired in positive ionization mode with nebulizing gas flow rate of 0.2 L min^{-1}, interface voltage at 2 kV, interface temperature at 58°C, and desolvation line (DL) temperature at 250°C. Selected reaction monitoring (SRM) was used for data acquisition by monitoring the precursor-product ion transitions as indicated in **Supplemental Table S2**. These instruments and conditions were used during method validation and application on CSF samples.

2.8 Method validation

Linearity and limit of detection Linearity was evaluated by preparing calibration lines (n = 3) on three consecutive days. The calibration ranges are shown in **Table 3.** All calibration lines were fitted to a $1/x^2$ weighted linear regression model. The limits of detection (LOD) and limits of quantification (LOQ) were calculated as LOD = 3 × S_a/b, LOQ = 10 × S_a/b, where S_a is the standard deviation of the y-intercept, b is the slope of the calibration curve [25].

Table 3. Validation parameters: calibration range, retention time, LODs, and LOQs.

Compound	Calibration ranges (pM)	Retention time (min)	R^2	LOD (pM)	LOQ (pM)
α-LEA	29.3-7500	10.0	0.9978	3.5	11.8
EPEA	58.6-7500	10.0	0.9980	15.1	50.4
POEA	14.6-7500	10.4	0.9970	2.6	8.7
PDEA	7.3-7500	10.8	0.9978	2.1	7.0
DHEA	58.6-7500	10.8	0.9963	34.4	114.6
AEA	7.3-7500	10.9	0.9982	0.7	2.4
LEA	29.3-7500	11.0	0.9983	14.8	49.3
DGLEA	29.3-7500	11.5	0.9975	2.0	6.5
1-AG/2-AG	146.5-75000	11.6/11.8	0.9965	0.6	2.0
1-LG/2-LG	1464.8-750000	11.7/11.9	0.9957	3.2	10.5
PEA	585.9-75000	11.7	0.9933	1293.4	4311.3
ETAEA	29.3-7500	11.9	0.9966	14.1	46.9
OEA	73.2-75000	12.0	0.9988	5.3	17.8
DEA	7.3-7500	12.1	0.9965	1.3	4.4
1-OG/2-OG	5859.4-750000	12.5/12.7	0.9976	45.7	152.4
SEA	146.5-75000	13.0	0.9963	29.5	98.3

*R^2, coefficient of determination.

Precision The intra- and interday precisions were evaluated by spiking three different concentrations of ISTD solutions [low-level(C2), medium-level(C4) and high-level(C6)] into pooled CSF samples over three different days (n = 3). Precision was expressed as the RSD of the peak areas of ISTD. An RSD less than 15% was within the tolerance limits of the EMA guidelines [24].

Recovery and matrix effects Recovery and matrix effect were evaluated by spiking ISTD solutions to pooled CSF samples (n = 3) or water (n = 3). Recovery was calculated as the ratio of ISTD peak areas measured before and after extraction. Matrix effect was the ratio of spiked ISTD peak areas acquired within pooled CSF and water, both spiked after extraction.

2.9 Data preprocessing

LabSolutions LCMS Version 5.97 SP1 (Shimadzu, Japan) and SCIEX OS version 1.6 (SCIEX, United States) were used for peak picking and integration. Absolute quantitation was calculated using the equation of the calibration curve and using the peak area ratios (peak area of targeted analyte divided by peak area of respective ISTD). F-test for linear regression was performed using Excel 2016.

3. Results and discussion

3.1 Optimization of micro-flow rates and comparison with UHPLC-MS

The main advantage of micro-LC is the ability to obtain similar or lower LODs compared with UHPLC, but with significantly reduced injection volumes, making this approach well-suited for analyzing compounds in biomass-restricted samples [26]. Another advantage of micro-LC is a higher robustness compared to nano-LC columns, which is key for clinical studies. In addition to the expected advantages of downscaling LC column diameters, such as higher sensitivity [27], micro-LC results in an improved ESI efficiency. Various flow rates were evaluated using direct infusion MS and micro-LC-MS analysis of eCBs to evaluate the improvement in ESI efficiency. With direct infusion, various flow rates at conventional (i.e., 550 µL min^{-1}, 250 µL min^{-1}, 100 µL min^{-1}) and micro-level (i.e., 4 µL min^{-1}, 3 µL min^{-1}, 2 µL min^{-1}, 1 µL min^{-1}) range were investigated, with optimized parameters on the same MS instrument. After allowing the flow rates to stabilize, a time

window of 1 min was picked and data within this window was summed. The sensitivity of each flow rate was expressed as counts per mole. As shown in **Figure 1**, significant improvements of the sensitivity were observed for both AEA and 2-AG as the flow rate decreased, especially at the low µL min^{-1} flow rates. This observation is in line with previously reported findings, in which the sensitivity improvement at lower flow rates was attributed to an improved ionization efficiency [28]. It is worth mentioning that, although the increasing trends were still sharp when the flow rate changed to 1 µL min^{-1}, a noticeable increase of background noise was also observed, which may affect the signal-to-noise ratio in the LC-MS analysis.

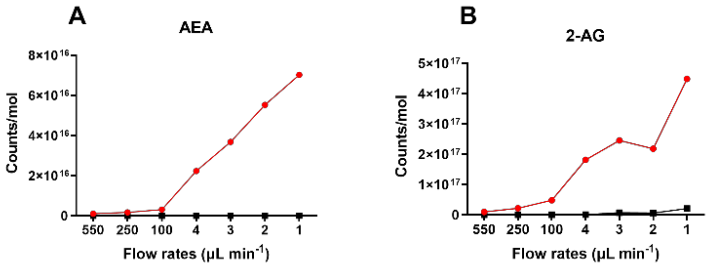

Figure 1. Effect of different flow rates on sensitivity of (A) AEA and (B) 2-AG with direct infusion to SCIEX Qtrap 6500+ with Sciex Turbo V ionization source (100-550 µL min-1) and NanosprayIII ionization source (1-4 µL min-1). Red line: infusion of standard solution I with 5 nM AEA and 50 nM 1-AG/2-AG in 70% ACN. Black line: infusion of blank sample containing 70% ACN. The y-axis shows the signal as counts per mol, x-axis shows flow rates. MS parameters are listed in **Supplemental Table S1**.

Subsequently, the effect of flow rates was investigated using three micro-LC columns of different inner diameters. Based on the column capacity, four different flow rates from 550 µL min^{-1} to 4 µL min^{-1} were investigated using three columns with inner diameters of 2.1 mm, 1 mm and 0.3 mm, respectively (**Table 2**). The injection volumes of standard solution II on the three columns were 10 µL, 5 µL, and 0.5 µL, respectively. The dilution fold of injected sample under micro-flow rate was smaller, therefore, higher concentration of samples reached the MS interface. **Figure 2A** shows that peak areas of all compounds significantly increased as the flow rates decreased. The detector response observed at each condition is expressed as the ratio of peak area to injection volume. As an example, at a

flow rate of 4 µL min^{-1}, the detector responses for AEA and 1-AG/2-AG were 9.7 and 9.4 times higher compared with responses observed at a flow rate of 550 µL min^{-1}, respectively. The sensitivity for eCB analogues improved 5 to 22 times. The results confirm that the ionization efficiency of eCBs and eCB analogues can be enhanced by down-scaling flow rates using suitable columns.

In conclusion, a micro-flow LC-MS/MS method was able to increase the sensitivity of eCBs compared to a conventional UHPLC-MS/MS method. The MS signal is proportional to the amount of compounds reaching the detector within each unit of time, which demonstrates that micro-flow LC-MS analysis is concentration-dependent [29], where the lower the flow rate, the higher the signal. However, the robustness of the micro-flow method, when it reaches 1 µL min^{-1} or even the nano-flow level is crucial to consider. After taking the capacity of column, cycle time of the analysis, sensitivity required for quantification and most importantly, the method robustness into account, 4 µL min^{-1} was selected for the following experiments.

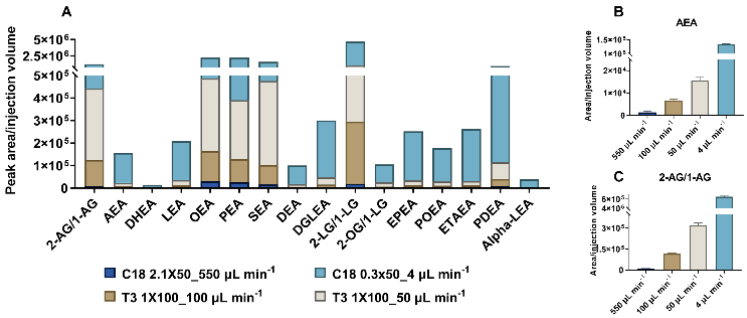

Figure 2. Effect of different flow rates on sensitivity of standard solution II with different I.D. columns. SCIEX QTRAP 6500+with SCIEX Turbo V ionization source (50 - 550 µL min^{-1}) and NanosprayIII ionization source (4 µL min^{-1}) was used. SCIEX QTRAP 6500+ with SCIEX Turbo V ionization source (50-550 µL min^{-1}) and NanosprayIII ionization source (4 µL min^{-1}) was used. LC-MS parameters can be found in **Table 2** and **Supplemental Table S1**. Sensitivity is shown on y-axis, expressed as the ratio of compounds peak area to injection volume. (A) Sensitivity of all the targeted compounds with different flow rates; (B) Sensitivity of AEA at different flow rates; (C) Sensitivity of 1-AG/2-AG at different flow rates.

3.2 Micro-LC-MS/MS method development

Clogging in the tubing or spray needle remains a major obstacle during the development of low-flow rate LC-MS methods [30]. To avoid clogging and improve the ionization efficiency of the developed micro-LC-MS/MS method, we modified the micro-spray needles on the Shimadzu 8060. In the original micro-ion source, Shimadzu used a design called "UF-link^{TM}". As shown in **Figure 3A** and **3C**, the original micro-spray needle consisted of a metal needle (opening I.D. = 50 μm) and peak tubing, which were glued together. By connecting the peek tubing directly to the separation column, the dead volume from the connections and extra tubing was minimized. However, during practical use, the glued part was constantly clogged even when using standard solution injections under micro-flow rates. Since the ion source otherwise gave satisfactory performance, we decided to optimize the spray needle to fix the problem. After modification, the whole tubing part including peek part and metal part was removed and replaced by a 15-cm Metal TaperTip emitter (30-μm tip opening and 360-μm outer diameter). This metal emitter was able to sustain robust performance for flow rates up to 5 μL min^{-1}. At micro-flow rates, the influence of the volume in post-column tubing and unions on peak shape, especially peak broadening, may be amplified. In this study, the spray emitter was connected to fused silica tubing (50 μm I.D., 60-cm length) with well-fitting sleeves and a zero dead volume union. Although the total add-on volume was around 1.2 μL, no significant peak broadening or shifting was observed during the analysis.

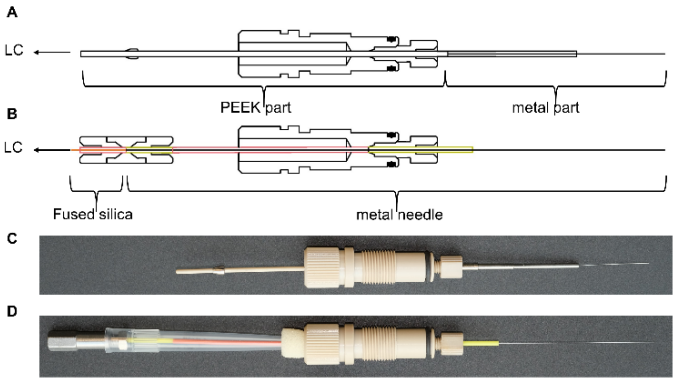

Figure 3. Illustration of (A) the original spray needle and (B) the optimized spray needle; Pictures of (C) original spray needle and (D) optimized spray needle.

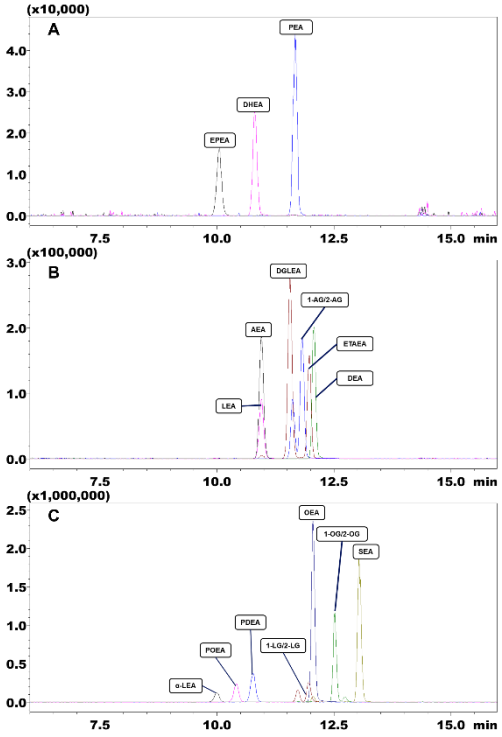

Figure 4. Overlay of SRM chromatograms of eCBs and eCB analogues obtained with the injection of standard solution II. The three panels represent the same chromatogram in different scales. (A) compounds with 1×10^4 scale intensity (B) compounds with 1×10^5 intensity scale (C) compounds with 1×10^6 intensity scale.

The micro-LC gradient was optimized based on previous work [19]. The injection volume was evaluated based on column capacity, signal intensity and peak shape. Initial mobile phase was used as injection solvent since it resulted in the best peak shape. Next, MS parameters including nebulizing gas, heating gas, interface temperature, interface voltage, collision energy and dwell time were further optimized with standard solution. The optimized LC-MS parameters are described in **Section 2.7**. After the optimization of micro-LC-MS/MS conditions, all the targeted compounds were separated with nice peak shape by using a Phenomenex C18 (2.6 μm, 0.3 × 150 mm) column with 16 minutes analysis time (**Figure 4**). Typical SRM chromatograms of targeted eCBs and eCB analogues in human CSF are shown in **Figure 5**. It is worth mentioning that due to the volume of mobile phase mixer, online filter, and tubings in micro-LC system, gradients could not reach the column

immediately at a flow rate of 4 µL min^{-1}, which results in a delay of the retention time. Such delay, however, will not affect the peak shape or method repeatability.

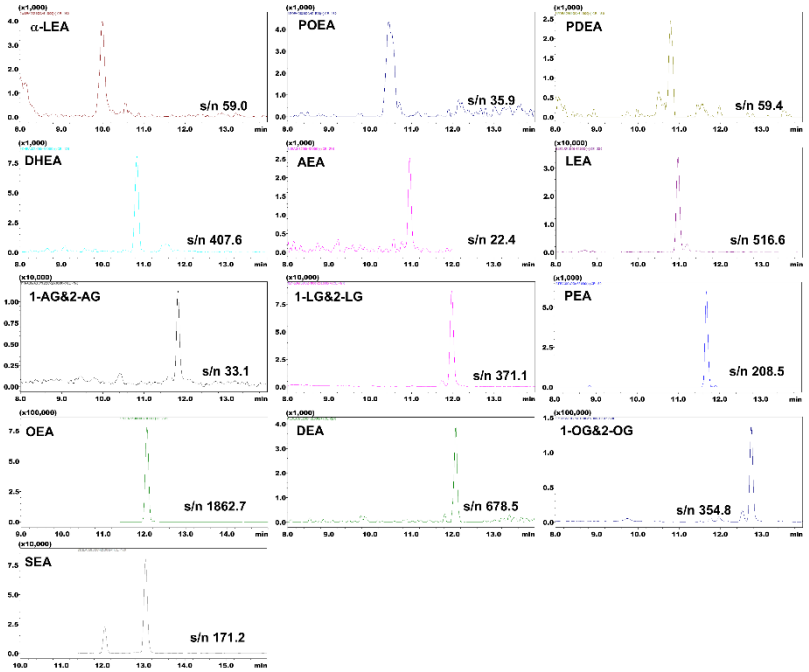

Figure 5. SRM chromatograms of eCBs and eCB analogues in pooled human CSF as determined by micro-LC-MS/MS using a flow rate of 4 µL min^{-1} and an injection volume of 3 µL. The x-axis is retention time and the y-axis is the detector response signal.

3.3 Analytical performance evaluation

The optimized method in **Section 2.7** was validated according to the EMA guidelines for the validation of analytical methods [24], with evaluation of linearity, precision, recovery and matrix effects. The calibration ranges were determined according to the levels observed in test samples as well as the information retrieved from the Human Metabolome Database (HMDB) and literature [11-17, 20, 31-34]. The linearity, LOD and LOQ are summarized in **Table 3**. Precision (intraday and interday) values, recovery and matrix effects are summarized in **Table 4**.

The coefficient of determination (R^2) values were all between 0.995 and 0.999 (significance F <0.05), and at least 75% of the back calculated concentrations of the calibration standards

were within ±15% (20% for LOQ) of the nominal value, indicating that the linearity was satisfactory for all the analytes. The LOQs were between 2.0 and 152.4 pM for most of the compounds, with the exception of PEA. A study reported that PEA contained in polyurethane foam, which is used for the wrapping material for some experimental glassware, can be absorbed by the glass and later on released to organic solvent during sample preparation [35]. Another report showed that plastic material could also be contaminated by NAEs including PEA [36]. It is important to monitor background contamination of this class to avoid jeopardizing the quantification accuracy of these compounds in biological samples. We observed noticeable PEA peaks in blank sample (50% ACN) and in the lowest calibrant of the calibration curve. Hence, the contamination of PEA from laboratory materials can explain its abnormally high LOD and LOQ values.

Table 4. Intraday and interday precision (RSD%).

compounds	Intraday precision (%)			Interday precision (%)		
	Low	Medium	High	Low	Medium	High
d_8-AEA	10.9%	0.3%	0.1%	13.7%	2.7%	3.8%
d_8-2-AG	3.2%	2.2%	4.6%	10.9%	9.6%	6.3%
d_4-OEA	9.8%	8.8%	2.3%	13.7%	6.7%	2.2%
d_4-LEA	0.3%	1.6%	2.3%	10.1%	5.4%	10.2%
d_4-DHEA	9.2%	5.5%	9.3%	10.1%	5.4%	10.2%
d_4-PEA	6.5%	6.2%	3.8%	11.0%	13.5%	6.4%
d_3-SEA	4.2%	0.9%	0.2%	6.1%	8.6%	5.7%

The intraday and interday precision were assessed using three different concentrations [low-level (C2), medium-level (C4), and high-level (C6)] of internal standards spiked in pooled CSF. Triplicate samples were prepared in each batch, and three batches were measured in three consecutive days. Intra- and interday precisions varied from 0.1% to 10.9% and from 2.2% to 13.7%, respectively, which are all within 15%, indicating that the repeatability was within the tolerance limits (**Table 4**). These results are comparable to previously reported quantification methods for eCBs with nano-flow LC-MS [19], as well as some methods with conventional LC-MS. In addition, during the analysis of the 288 CSF samples, no significant signal decrease was observed, which also demonstrated the robustness of this method.

Recovery and matrix effect were determined using deuterated internal standards. The recoveries ranged from 61.5% to 114.8%. Matrix effects ranged from 24.4% to 105.2% (**Figure 6**). All compounds showed acceptable recovery. Major matrix effects were observed for several analytes, which may be caused by co-eluting phospholipids. As deuterated ISTDs were used, the quantification accuracy was ensured.

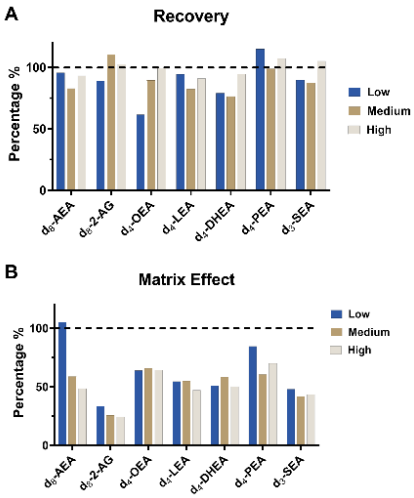

Figure 6. Recovery and matrix effect of deuterated internal standards in human CSF. Recovery and matrix effect values are expressed in percentages. (A) Recovery: higher values indicate better recoveries. (B) Matrix effect: values above 100% imply ion enhancement and below 100% imply ion suppression.

3.4 Application to the analysis of human CSF samples

As part of another study, CSF samples were collected in a population of males and females with an age ranging from 18 to 69 and measured using the developed micro-LC-MS/MS method. The study was conducted according to the criteria of the Declaration of Helsinki and was approved by the Leiden University Medical Center institutional ethics committee. All participants provided written informed consent prior to participation in the study. Data obtained from the heathy controls (n = 94) is reported in current study. The concentration distributions of AEA and 2-AG in the 94 healthy control samples and their correlation with gender and age are shown in **Figure 7**. Concentration of AEA in this CSF study for healthy controls ranged from 1.0-7.1 pM, and for 2-AG from 87.9-658.5 pM. These levels can be

used as future reference in follow-up studies. Significant correlation was observed between age and 2-AG concentration in healthy females (p-value = 0.026). However, no clear correlation was observed between age and the concentration of AEA in human CSF. Although it should be noted that confounding factors might have affected the relation as we did not take these into account. Moreover, the quantification results showed that this method is robust and sensitive enough to be applied to future clinical studies.

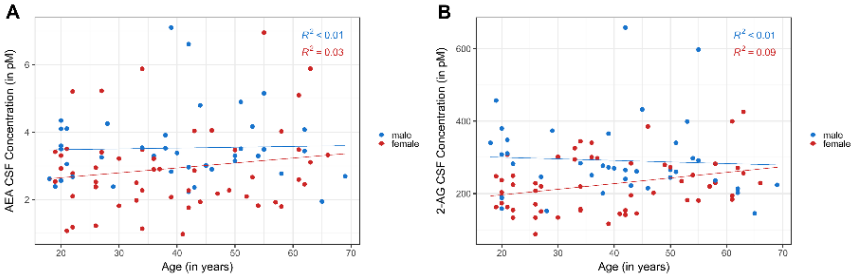

Figure 7. Correlation between compounds and age based on the quantification data using the validated micro-LC-MS/MS method. The colors represent male (blue) and female (red). R^2 = coefficient of determination.

4 Conclusion

In this study, we developed and optimized a novel micro-LC-MS/MS method for the determination of eCBs and their analogues in human CSF. By using AEA and 1-AG/2-AG as reference compounds, the comparison of conventional and micro-level flow rates highlighted the advantage of micro-flow in increasing the sensitivity for targeted compounds. The flow rate was down scaled to 4 µL min^{-1} with a 0.3-mm inner diameter column, other setting and parameters were also optimized correspondingly to adapt the micro-flow. A minor modification on Shimadzu Mikros Micro-ESI spray needle was carried out to improve the robustness of this method. Requiring 250 µL CSF, the method reached LODs ranging from 0.6 to 1293.4 pM and LOQs ranging from 2.0 to 4311.3 pM. The repeatability was within the tolerance limits, with intraday and interday precisions under 13.7%. The developed micro-LC-MS/MS method was found to be fit-for-purpose for the analysis of clinical CSF samples, in which 288 human CSF samples were successfully measured. With the wider coverage of eCBs and high robustness for CSF analysis, our

method showed its applicability for future clinical research of brain disorders in which a disturbance in the ECS can be expected.

Declaration of Competing Interest

The authors declare that they have no known competing financial interests or personal relationships that could have appeared to influence the work reported in this paper.

Acknowledgements

This study was supported by the China Scholarship Council (CSC, No. 201906390032 to Bingshu He and CSC, No. 201707060012 to Xinyu Di). Dr. Rawi Ramautar would like to acknowledge the financial support of the Vidi grant scheme of the Netherlands Organization of Scientific Research (NWO Vidi 723.016.003). This work was also supported by the Netherlands Organization for Health Research and Development (Vidi grant no. 917-11-31 to GMT), and European Community (EC) funded FP7-EUROHEADPAIN (grant no. 602633 to AMJMvdM). This research was part of the Netherlands X-omics Initiative and partially funded by NWO, project 184.034.019.

References

[1] F.A. Iannotti, V. Di Marzo, S. Petrosino, Endocannabinoids and endocannabinoid-related mediators: Targets, metabolism and role in neurological disorders, Progress in Lipid Research, 62 (2016) 107-128.
[2] S. Ben-Shabat, E. Fride, T. Sheskin, T. Tamiri, M.-H. Rhee, Z. Vogel, T. Bisogno, L. De Petrocellis, V. Di Marzo, R. Mechoulam, An entourage effect: inactive endogenous fatty acid glycerol esters enhance 2-arachidonoyl-glycerol cannabinoid activity, European Journal of Pharmacology, 353 (1998) 23-31.
[3] W.-S. Ho, D.A. Barrett, M.D. Randall, 'Entourage' effects of N-palmitoylethanolamide and N-oleoylethanolamide on vasorelaxation to anandamide occur through TRPV1 receptors, British Journal of Pharmacology, 155 (2008) 837-846.
[4] R. Greco, C. Demartini, M. Francavilla, A.M. Zanaboni, C. Tassorelli, Dual Inhibition of FAAH and MAGL Counteracts Migraine-like Pain and Behavior in an Animal Model of Migraine, Cells, 10 (2021) 2543.
[5] A. Della Pietra, R. Giniatullin, J.R. Savinainen, Distinct Activity of Endocannabinoid-Hydrolyzing Enzymes MAGL and FAAH in Key Regions of Peripheral and Central Nervous System Implicated in Migraine, Int J Mol Sci, 22 (2021) 1204.
[6] E. Kilinc, S. Ankarali, I.E. Torun, Y. Dagistan, Receptor mechanisms mediating the anti-neuroinflammatory effects of endocannabinoid system modulation in a rat model of migraine, European Journal of Neuroscience, n/a.

[7] C. Tassorelli, R. Greco, S.D. Silberstein, The endocannabinoid system in migraine: from bench to pharmacy and back, Current Opinion in Neurology, 32 (2019) 405-412.
[8] J. Mulder, M. Zilberter, S.J. Pasquaré, A. Alpár, G. Schulte, S.G. Ferreira, A. Köfalvi, A.M. Martín-Moreno, E. Keimpema, H. Tanila, M. Watanabe, K. Mackie, T. Hortobágyi, M.L. de Ceballos, T. Harkany, Molecular reorganization of endocannabinoid signalling in Alzheimer's disease, Brain, 134 (2011) 1041-1060.
[9] C. Altamura, M. Ventriglia, M.G. Martini, D. Montesano, Y. Errante, F. Piscitelli, F. Scrascia, C. Quattrocchi, P. Palazzo, S. Seccia, F. Vernieri, V. Di Marzo, Elevation of Plasma 2-Arachidonoylglycerol Levels in Alzheimer's Disease Patients as a Potential Protective Mechanism against Neurodegenerative Decline, Journal of Alzheimer's Disease, 46 (2015) 497-506.
[10] P. Leimuranta, L. Khiroug, R. Giniatullin, Emerging Role of (Endo)Cannabinoids in Migraine, Front Pharmacol, 9 (2018).
[11] M. Di Filippo, L.A. Pini, G.P. Pelliccioli, P. Calabresi, P. Sarchielli, Abnormalities in the cerebrospinal fluid levels of endocannabinoids in multiple sclerosis, Journal of Neurology, Neurosurgery & Psychiatry, 79 (2008) 1224-1229.
[12] K.R. Müller-Vahl, L. Bindila, B. Lutz, F. Musshoff, T. Skripuletz, C. Baumgaertel, K.-W. Sühs, Cerebrospinal fluid endocannabinoid levels in Gilles de la Tourette syndrome, Neuropsychopharmacology, 45 (2020) 1323-1329.
[13] J. Nicholson, S. Azim, M.J. Rebecchi, W. Galbavy, T. Feng, R. Reinsel, S. Rizwan, C.J. Fowler, H. Benveniste, M. Kaczocha, Leptin levels are negatively correlated with 2-arachidonoylglycerol in the cerebrospinal fluid of patients with osteoarthritis, PloS one, 10 (2015) e0123132-e0123132.
[14] P. Sarchielli, L.A. Pini, F. Coppola, C. Rossi, A. Baldi, M.L. Mancini, P. Calabresi, Endocannabinoids in Chronic Migraine: CSF Findings Suggest a System Failure, Neuropsychopharmacology, 32 (2007) 1384-1390.
[15] R. Jumpertz, A. Guijarro, R.E. Pratley, D. Piomelli, J. Krakoff, Central and Peripheral Endocannabinoids and Cognate Acylethanolamides in Humans: Association with Race, Adiposity, and Energy Expenditure, The Journal of Clinical Endocrinology & Metabolism, 96 (2011) 787-791.
[16] A. Romigi, M. Bari, F. Placidi, M.G. Marciani, M. Malaponti, F. Torelli, F. Izzi, C. Prosperetti, S. Zannino, F. Corte, C. Chiaramonte, M. Maccarrone, Cerebrospinal fluid levels of the endocannabinoid anandamide are reduced in patients with untreated newly diagnosed temporal lobe epilepsy, Epilepsia, 51 (2010) 768-772.
[17] C. Marchioni, B.L. Santos-Lobato, M.E.C. Queiroz, J.A.S. Crippa, V. Tumas, Endocannabinoid levels in patients with Parkinson's disease with and without levodopa-induced dyskinesias, Journal of Neural Transmission, 127 (2020) 1359-1367.
[18] J. Nicholson, S. Azim, M.J. Rebecchi, W. Galbavy, T. Feng, R. Reinsel, S. Rizwan, C.J. Fowler, H. Benveniste, M. Kaczocha, Leptin levels are negatively correlated with 2-arachidonoylglycerol in the cerebrospinal fluid of patients with osteoarthritis, PloS one, 10 (2015) e0123132.
[19] V. Kantae, S. Ogino, M. Noga, A.C. Harms, R.M. van Dongen, G.L.J. Onderwater, A.M.J.M. van den Maagdenberg, G.M. Terwindt, M. van der Stelt, M.D. Ferrari, T. Hankemeier, Quantitative profiling of endocannabinoids and related N-acylethanolamines in human CSF using nano LC-MS/MS, Journal of Lipid Research, 58 (2017) 615-624.
[20] J. Czepiel, J. Gdula-Argasińska, G. Biesiada, B. Bystrowska, A. Jurczyszyn, W. Perucki, K. Sroczyńska, A. Zając, T. Librowski, A. Garlicki, Fatty acids and selected endocannabinoids content in cerebrospinal fluids from patients with neuroinfections, Metab Brain Dis, 34 (2019) 331-339.
[21] F.M. Leweke, A. Giuffrida, D. Koethe, D. Schreiber, B.M. Nolden, L. Kranaster, M.A. Neatby, M. Schneider, C.W. Gerth, M. Hellmich, J. Klosterkötter, D. Piomelli, Anandamide levels in cerebrospinal fluid of first-episode schizophrenic patients: Impact of cannabis use, Schizophrenia Research, 94 (2007) 29-36.
[22] A.E. Kirby, M.J. Jebrail, H. Yang, A.R. Wheeler, Folded emitters for nanoelectrospray ionization mass spectrometry, Rapid Communications in Mass Spectrometry, 24 (2010) 3425-3431.
[23] Y. Huang, Q. Zhang, Y. Liu, B. Jiang, J. Xie, T. Gong, B. Jia, X. Liu, J. Yao, W. Cao, H. Shen, P. Yang, Aperture-controllable nano-electrospray emitter and its application in cardiac proteome analysis, Talanta, 207 (2020) 120340.
[24] E.E.M. Agency, Guidlines for the validation of analytical methods used in residue depletion studies, in: E.M. Agency (Ed.), 2009.
[25] A. Shrivastava, V.B. Gupta, Methods for the Determination of Limit of Detection and Limit of Quantitation of the Analytical Methods, Chron Young Sci, 2 (2011) 15-21.
[26] J. Zhang, W. Shou, T. Ogura, S. Li, H. Weller, Optimization of microflow LC–MS/MS and its utility in quantitative discovery bioanalysis, Bioanalysis, 11 (2019) 1117-1127.

[27] M. Hilhorst, C. Briscoe, N.v.d. Merbel, Sense and nonsense of miniaturized LC–MS/MS for bioanalysis, Bioanalysis, 6 (2014) 3263-3265.
[28] A. Schmidt, M. Karas, T. Dülcks, Effect of different solution flow rates on analyte ion signals in nano-ESI MS, or: when does ESI turn into nano-ESI?, Journal of the American Society for Mass Spectrometry, 14 (2003) 492-500.
[29] H. Liu, G. Raffin, G. Trutt, J. Randon, Is vacuum ultraviolet detector a concentration or a mass dependent detector?, Journal of Chromatography A, 1530 (2017) 171-175.
[30] K.L. Sanders, J.L. Edwards, Nano-liquid chromatography-mass spectrometry and recent applications in omics investigations, Analytical Methods, 12 (2020) 4404-4417.
[31] M. Bobrich, R. Schwarz, R. Ramer, P. Borchert, B. Hinz, A simple LC-MS/MS method for the simultaneous quantification of endocannabinoids in biological samples, Journal of Chromatography B, 1161 (2020) 122371.
[32] I. Mennella, M. Savarese, R. Ferracane, R. Sacchi, P. Vitaglione, Oleic acid content of a meal promotes oleoylethanolamide response and reduces subsequent energy intake in humans, Food & Function, 6 (2015) 203-209.
[33] R. Ottria, A. Ravelli, F. Gigli, P. Ciuffreda, Simultaneous ultra-high performance liquid chromathograpy-electrospray ionization-quadrupole-time of flight mass spectrometry quantification of endogenous anandamide and related N-acylethanolamides in bio-matrices, Journal of Chromatography B, 958 (2014) 83-89.
[34] P.J.H. Jones, L. Lin, L.G. Gillingham, H. Yang, J.M. Omar, Modulation of plasma N-acylethanolamine levels and physiological parameters by dietary fatty acid composition in humans, Journal of lipid research, 55 (2014) 2655-2664.
[35] Identification of a Widespread Palmitoylethanolamide Contamination in Standard Laboratory Glassware, Cannabis and Cannabinoid Research, 2 (2017) 123-132.
[36] S. Oddi, F. Fezza, G. Catanzaro, C. De Simone, M. Pucci, D. Piomelli, A. Finazzi-Agro , M. Maccarrone, Pitfalls and solutions in assaying anandamide transport in cells[S], Journal of Lipid Research, 51 (2010) 2435 - 2444.

Supplementary Material

Table S1(A). MS parameters of SCIEX QTRAP 6500+ mass spectrometer used in flow rate evaluation experiment.

	Conventional flow		**Micro flow**					
Flow rates	550 µL min^{-1}	250 µL min^{-1}	100 µL min^{-1}	50 µL min^{-1}	4 µL min^{-1}	3 µL min^{-1}	2 µL min^{-1}	1 µL min^{-1}
Curtain gas	30	30	20	20	20	20	20	20
Ionspray voltage	5500	5500	4700	4700	2400	2300	2200	2100
Ion source gas 1	50	50	30	30	10	10	10	10
Ion source gas 2	50	50	30	0	0	0	0	0
Interface heater temperature	600	600	450	450	150	140	120	100
DP	50	50	50	50	50	50	50	50
EP	12	12	12	12	12	12	12	12
CXP	11	11	11	11	11	11	11	11

Table S1(B). LC gradients in LC-MS flow rates comparison.

Flow rate	**550 µL min^{-1}**		**Flow rate**	**100 µL min^{-1} and 50 µL min^{-1}**		**Flow rate**	**4 µL min^{-1}**	
Time (min)	A[%]	B[%]	Time (min)	A[%]	B[%]	Time (min)	A[%]	B[%]
0	45	55	0	45	55	0	45	55
0.5	45	55	0.5	45	55	0.5	45	55
1.5	40	60	2	40	60	2	40	60
2	30	70	2.5	30	70	2.5	30	70
5.5	15	85	7.5	15	85	7.5	15	85
5.6	5	95	8	5	95	8	5	95
8	5	95	10	5	95	10	5	95
8.1	45	55	10.1	45	55	10.1	45	55
10	45	55	12	45	55	16	45	55

Table S2. MRM (Multiple reaction monitoring) parameters of the target compounds with Shimadzu 8060 mass spectrometer.

Compound name	ChEBI ID	Abbreviation	Molecular formula	MW g/mole	Precursor ion (m/z)	Product ion (m/z)	Dwell time (msec)	CE
α-Linolenoyl ethanolamide	89605	a-LEA	$C_{20}H_{35}NO_2$	325.5	322.4	61.9	20	-16
Palmitoleoyl ethanolamide	71465	POEA	$C_{18}H_{35}NO_2$	297.5	298.4	62.2	5	-16
Pentadecanoyl ethanolamide	165589	PDEA	$C_{17}H_{35}NO_2$	285.5	386.4	61.9	5	-15
Linoleoyl ethanolamide	64032	LEA	$C_{20}H_{37}NO_2$	323.5	324.3	62	20	-33
Anandamide	2700	AEA	$C_{22}H_{37}NO_2$	347.5	348.2	62.0	20	-23
Docosahexaenoyl ethanolamide	85252	DHEA	$C_{24}H_{37}NO_2$	371.6	372.4	62	20	-17
1-Arachidonoylglycerol / 2-Arachidonoylglycerol	75612 52392	1-AG/2-AG[a]	$C_{23}H_{38}O_4$	378.5	379.2	287.0	20	-15
1-Linoleoyl glycerol / 2-Linoleoyl glycerol	75565 173124	1-LG/2-LG[b]	$C_{21}H_{38}O_4$	354.5	355.1	263.0	10	-17
Palmitoyl ethanolamide	71464	PEA	$C_{18}H_{37}NO_2$	299.5	300.4	62.0	5	-5
Dihomo-γ-linolenoyl ethanolamide	34488	DGLEA	$C_{22}H_{39}NO_2$	349.5	350.2	62	5	-17
Docosatetraenoyl ethanolamide	34478	DEA	$C_{24}H_{41}NO_2$	375.6	376.2	62.0	8	-22
1-Oleoyl glycerol / 2-Oleoyl glycerol	75342 73990	1-OG/2-OG[c]	$C_{21}H_{40}O_4$	356.5	357.3	265.3	10	-12
Stearoyl ethanolamide	85299	SEA	$C_{20}H_{41}NO_2$	327.5	328.3	62.0	5	-17
Eicosapentaenoyl ethanolamide	71467	EPEA	$C_{22}H_{35}NO_2$	345.5	346.2	61.9	20	-16
Mead acid ethanolamide	165588	ETAEA	$C_{22}H_{39}NO_2$	349.5	350.2	62	5	-17
N-Oleoylethanolamine	71466	OEA	$C_{20}H_{39}NO_2$	325.5	326.0	62.0	20	-22
N-linoleoylethanolamide - d_4		d_4-LEA-ISTD	$C_{20}H_{33}D_4NO_2$	327.5	328.3	66.2	20	-33
N-docosahexaenoyl ethanolamide- d_4		d_4-DHEA-ISTD	$C_{24}H_{33}D_4NO_2$	375.6	376.3	66.2	10	-17
N-arachidonoyl ethanolamide - d_8		d_8-AEA-ISTD	$C_{22}H_{29}D_8NO_2$	355.6	356.3	62.0	20	-23
N-arachidonoylglycerol - d_8		d_8-2-AG-ISTD	$C_{23}H_{30}D_8O_4$	386.6	387.3	294.2	20	-15
N-palmitoylethanolamide - d_4		d_4-PEA-ISTD	$C_{18}H_{33}D_4NO_2$	303.5	304.4	62.0	5	-5
N-oleoylethanolamide - d_4		d_4-OEA-ISTD	$C_{20}H_{35}D_4NO_2$	329.6	330.0	66.0	8	-22
N-stearoylethanolamide - d_3		d_3-SEA-ISTD	$C_{20}H_{38}D_3NO_2$	330.6	331.3	62.0	5	-17

Table S3. Accuracy and precision at lowest points of calibration curves (n=3).

Compound	Calibration ranges (pM)	Retention time (min)	R^2	Nominal concentration (pM)	Calculate concentration (pM)	Accuracy	Precision
α-LEA	29.3-7500	10.0	0.9978	29.3	27.7	94.4%	6.3%
EPEA	58.6-7500	10.0	0.9980	58.6	57.7	98.5%	5.5%
POEA	14.6-7500	10.4	0.9970	14.6	14.5	99.2%	17.8%
PDEA	7.3-7500	10.8	0.9978	7.3	6.9	93.6%	12.4%
DHEA	58.6-7500	10.8	0.9963	58.6	61.4	104.7%	2.8%
AEA	7.3-7500	10.9	0.9982	7.3	6.9	94.6%	6.8%
LEA	29.3-7500	11.0	0.9983	29.3	28.5	97.2%	13.4%
DGLEA	29.3-7500	11.5	0.9975	29.3	25.0	85.3%	5.6%
1-AG/2-AG	146.5-75000	11.6/11.8	0.9965	146.5	159.9	109.1%	1.2%
1-LG/2-LG	1464.8-750000	11.7/11.9	0.9957	1464.8	1528.2	104.3%	5.5%
PEA	585.9-75000	11.7	0.9933	585.9	661.1	112.8%	3.6%
ETAEA	29.3-7500	11.9	0.9966	29.3	26.1	89.2%	2.9%
OEA	73.2-75000	12.0	0.9988	73.2	83.2	113.6%	3.0%
DEA	7.3-7500	12.1	0.9965	7.3	7.7	105.6%	12.6%
1-OG/2-OG	5859.4-750000	12.5/12.7	0.9976	5859.4	5747.1	98.1%	4.7%
SEA	146.5-75000	13.0	0.9963	146.5	174.2	118.9%	3.5%

*Accuracy = calculate concentration / nominal concentration × 100%;

Precision = RSD% of calculate concentration